

1 **QUANTIFYING THE RESPONSE OF**
2 **BLAINVILLE’S BEAKED WHALES TO US NAVAL**
3 **SONAR EXERCISES IN HAWAII**

4
5 **Eiren K. Jacobson¹, E. Elizabeth Henderson², David L. Miller¹, Cornelia S.**
6 **Oedekoven¹, David J. Moretti³, Len Thomas¹**

7 ¹ *Centre for Research into Ecological and Environmental Modelling, School of Mathematics and*
8 *Statistics, University of St Andrews, St Andrews, Scotland*

9 ² *Naval Information Warfare Center Pacific, San Diego, CA, USA*

10 ³ *Naval Undersea Warfare Center, Newport, RI, USA*

11 **Correspondence:**

12 Eiren Jacobson
13 University of St Andrews
14 The Observatory
15 Buchanan Gardens
16 St Andrews
17 Fife
18 KY16 9LZ
19 Scotland
20 Email: eiren.jacobson@st-andrews.ac.uk

21 **Draft 02 April 2021**
22

Abstract

Behavioral responses of beaked whales (family Ziphiidae) to naval use of mid-frequency active sonar (MFAS) have been quantified for some species and regions. We describe the effects of MFAS on the probability of detecting diving groups of Blainville's beaked whales (BBWs) on the US Navy Pacific Missile Range Facility (PMRF) in Hawaii and compare our results to previously published results for the same species in a different ocean basin. We used passive acoustic data collected at bottom-mounted hydrophones before and during six naval training exercises at PMRF along with modelled sonar received levels to describe the effect of training and MFAS on foraging groups of BBWs. We used a multi-stage generalized additive modelling approach to control for the underlying spatial distribution of vocalizations under baseline conditions. At a MFAS received level of 150 dB re $1\mu\text{Pa}$ the probability of detecting groups of BBWs decreased by 78% (95% CI 62%-100%) when compared to periods when general training activity was ongoing and by 92% (95% CI 87%-100%) when compared to baseline conditions. Our results indicate a more pronounced response to naval training and MFAS than has been previously reported. [187/200]

KEYWORDS

Blainville's beaked whales, *Mesopododon densirostris*, mid-frequency active sonar, passive acoustic data, behavioral response, generalized additive model

1 Introduction

Beaked whales (family Ziphiidae) are a group of deep-diving cetaceans that rely on sound to forage, navigate, and communicate (Aguilar de Soto et al., 2012; Johnson, Madsen, Zimmer, Aguilar de Soto, and Tyack, 2004; Macleod and D’Amico, 2006). Multiple mass strandings of beaked whales have been associated with high-intensity anthropogenic sound sources. These acute events have motivated research into whether and how beaked whales respond to different types and intensities of anthropogenic noise (Cox et al., 2006).

Anthropogenic sound can disrupt the patterned foraging dive cycles of beaked whales (Falcone et al., 2017), potentially leading to cumulative sublethal impacts resulting from reduced foraging opportunities (New, Moretti, Hooker, Costa, and Simmons, 2013), or to symptoms similar to decompression sickness that can lead to injury or death (Bernaldo de Quirós et al., 2019). For example, research on Blainville’s beaked whales (*Mesoplodon densirostris*) on a US Navy range in the Bahamas has shown that animals may stop foraging and/or move away from naval sonar sources (Joyce et al., 2019; Tyack et al., 2011).

Naval sonar can be broadcast from various platforms, including vessels, helicopters, buoys, submarines, and torpedoes (Harris et al., 2019; U.S. Department of the Navy, 2018). Most research has focused on the impacts of mid-frequency active sonar (MFAS) broadcast from naval vessels. Separately, researchers have shown that, in the absence of MFAS, beaked whales may alter their behavior in response to vessel noise (Aguilar de Soto et al., 2006; Pirotta et al., 2012).

The U.S. Navy is interested in quantifying the effects of sonar on beaked whales for the purpose of risk assessments and permitting associated with training activities (e.g., U.S. Department of the Navy, 2017). There are different experimental and analytical ways of quantifying responses to sonar. Here, we focus on analyses of data from cabled hydrophone arrays.

Examples of these from previous studies include McCarthy et al. (2011) who used data from the cabled hydrophone array at the US Navy’s Atlantic Undersea Test and Evaluation Center (AUTEC) in the Bahamas collected before, during, and after naval training exercises involving MFAS. The authors used separate generalized additive models (GAMs) for each period, and modelled the acoustic detection of groups of Blainville’s beaked whales (group vocal periods; GVPs) as a function of location on the range and time. They found that the number of GVPs was lower during the exercises than before or after.

Building on this work, Moretti et al. (2014) used a GAM to model the presence or absence of GVP starts within 30-min periods on the AUTEC range as a smooth function of MFAS received level. They compared the expected probability of detecting animals when no sonar was present to the expected probability of detecting animals across sonar received levels to estimate the probability of disturbance. They found that the probability of detecting groups of Blainville’s beaked whales was reduced by 50% at 150 dB re $1\mu\text{Pa}$, which they interpreted as a 50% probability of disturbance.

Our primary objective was to replicate the effort of Moretti et al. (2014) with the same species on a different US Navy training range in a different oceanic environment. We used a spatially-referenced dataset of Blainville’s beaked whale foraging dives recorded at the PMRF off the island of Kauai, Hawaii (Fig. 1). Acoustic detections of GVP starts within 30-min periods were collected via a cabled hydrophone array at PMRF before and during training exercises involving MFAS broadcast from navy ships.

Unlike AUTEC, which is situated in a deep isolated basin surrounded by steep slopes, the Pacific Missile Range Facility (PMRF) in Hawaii is located on the side of an ancient volcano, with a steep slope to the deep ocean floor. Previous work in this region has shown that Blainville’s beaked whales are present year-round at this site, prefer sloped habitats, and that acoustic detections decrease during multi-day training events involving MFAS (Henderson, Martin, Manzano-Roth, and Matsuyama, 2016; Manzano-Roth, Henderson, Martin, Martin,

and Matsuyama, 2016). As we expected the density of Blainville’s beaked whales at PMRF to be lower and more variable than at AUTEK (REF NEEDED), our methods needed to explicitly account for differences in underlying beaked whale presence across the range. An additional objective was to isolate the effect of general training activity from the effect of MFAS, so that beaked whale response to MFAS could be quantified relative to pre-training baseline periods and to periods when general training activities were present on the range. To this end, we fitted a series of three linked models.

2 Methods

2.1 Data Collection and Processing

2.1.1 Acoustic detection of beaked whales

The Pacific Missile Range Facility (PMRF) is an instrumented U.S. Naval range extending 70 km NW of the island of Kauai, Hawaii and encompassing 2,800 km². The range includes a cabled hydrophone array (Fig. 1) with hydrophones at depths ranging from approximately 650 m to 4,700 m. We used data collected before and during six Submarine Command Courses (SCCs) at PMRF. SCCs are training exercises that occur biannually in February and August and typically last 6-7 days. Acoustic recordings were made for a minimum of two days before each SCC as well as during the exercise. During data collection, hydrophones sampled at a rate of 96 kHz, with the high pass filter on each hydrophone set at 50 Hz, 100 Hz, or 10 kHz. Up to 62 hydrophones were recorded simultaneously by the Naval Information Warfare Center (NIWC).

A beaked whale detector from the Navy Acoustic Range WHale AnaLysis (NARWHAL) algorithm suite (C. R. Martin et al., 2020) was run on the recordings. This detector first compared signal-to-noise ratio (SNR) thresholds within the expected frequency range of

115 beaked whale clicks (16-44 kHz) versus the bandwidth outside the click in a running 16,384-
116 pt fast Fourier transform (FFT) spectrogram. The detected clicks were then passed to
117 a 64-pt FFT stage that measured power, bandwidth, slope, and duration characteristics
118 to classify the clicks to species. This process was followed by an automated routine in
119 MATLAB (*MATLAB*, 2017) to group detections of individual beaked whale echolocation
120 clicks into GVPs (Henderson et al., 2016). If a group of whales was detected by more than
121 one hydrophone, the GVP was assigned to the hydrophone that recorded the most clicks.
122 The data were then aggregated to indicate the presence or absence of the start of a GVP for
123 each hydrophone within each half-hour period.



Figure 1: Map of recorded hydrophones (black points) at the Pacific Missile Range Facility near the island of Kauai, Hawaii. For security reasons, the approximate rather than exact locations are shown here. Color scale indicates bathymetry. Inset map shows range location (black rectangle) relative to the main Hawaiian Islands.

2.1.2 Modelling received levels of hull-mounted mid-frequency active sonar

For security reasons, classified data regarding activity that occurred on the range during each SCC was passed from PMRF to one author with clearance (E.E.H.). These data indicated the locations of the ships during the training periods and the start and stop times of each individual training event. However, no information was provided on the start and stop of sonar use; hence, periods of active sonar were determined from the range hydrophone

130 recordings by running a sonar detector from the NARWHAL algorithm suite tuned to MFAS.
 131 The hydrophone recordings cannot be reliably used to determine received level when the
 132 received level exceeds 150 dB re. $1 \mu \text{ Pa}$. Additionally, the hydrophones are mostly 4-5
 133 km deep, whereas Blainville's beaked whales begin clicking when they have reached depths
 134 of approximately 200-500 m and spend most of their foraging dive at depths of 1-1.5 km
 135 (Johnson et al., 2004, Johnson, Madsen, Zimmer, Soto, and Tyack (2006), Madsen, Aguilar
 136 de Soto, Arranz, and Johnson (2013)). Therefore, we used propagation modelling to estimate
 137 transmission loss and calculate the expected maximum received level of hull-mounted MFAS
 138 around the location of each hydrophone at a depth of 1,000 m. First, the locations of
 139 all surface ships were noted at the start of each half-hour period and the closest ship to
 140 each hydrophone was determined. MFAS propagation was modelled using the parabolic
 141 equation propagation model in the program Peregrine (OASIS; Heaney and Campbell, 2016).
 142 Transmission loss was estimated using a 200 Hz band around the center frequency of the
 143 sonar (3.5 kHz). A nominal source level of 235 dB re. $1 \mu \text{ Pa}$ @ 1 m was assumed. The
 144 transmission loss was estimated along the radial from the ship to the hydrophone from a
 145 distance of 1 km before the hydrophone to 1 km past the hydrophone in 200 m increments and
 146 converted to received levels based on the source level of the sonar. The maximum modeled
 147 received level along that radial was determined for each hydrophone and half-hour period.
 148 However, if the distance between the ship and the hydrophone was less than the depth of
 149 the water column, the parabolic equation would overestimate transmission loss at that angle.
 150 In these cases, a simple sonar equation was used to estimate transmission loss instead. For
 151 hydrophones shallower than 1,000 m the received level was estimated at a point 20 m above
 152 the sea floor with a ± 10 m buffer, while for hydrophones deeper than 1,000 m the received
 153 level was estimated at a depth of 1,000 m with a ± 10 m buffer. This process resulted in
 154 an estimate of received level for each hydrophone and half-hour period. Uncertainty in the
 155 modeled received levels was not considered.

2.2 Spatial Modelling

2.2.0.1 Summary

We used a three-stage GAM approach to control for the underlying spatial distribution of Blainville’s beaked whales when modelling the effects of training activities and of MFAS. We first used tessellation to determine the area effectively monitored by each hydrophone. For the first model, we used pre-activity data to create a spatial model of the probability of GVPs across the range prior to the onset of naval activity. We used the predicted values from this first model as an offset in a second model created using data from when naval activity was present on the range, but MFAS was not. We then used the predicted values from this second model as an offset in a third model created using data when naval activity and MFAS were present on the range. Finally, we used posterior simulation to calculate confidence intervals and quantified the change in the probability of detecting GVPs when naval activity was present and across received levels of MFAS.

2.2.1 Determining hydrophone effort

For security reasons, randomly jittered locations and depths of hydrophones at PMRF were used. We projected the coordinates of each hydrophone into Universal Transverse Mercator Zone 4. Because the beaked whale detection algorithm assigned GVPs to the hydrophone that recorded the most echolocation clicks, and because the spatial separation of the hydrophones was not uniform, effort was not the same for all hydrophones. This meant that some hydrophones may have detected more GVPs because they were further away from other hydrophones, not because they were located in higher-density areas. To account for this, we used a Voronoi tessellation implemented in the R (R Core Team, 2018) package `deldir` (Turner, 2019) to define a tile for each hydrophone that contained all points on the range that were closest to that hydrophone. We assumed that beaked whale groups occur within the tessellation tile of the hydrophone to which the GVP is assigned, and that the area of

each tessellation tile influences the GVP detection rate at that hydrophone. For hydrophones on the outside of the range, i.e., not surrounded by other hydrophones, we used a cutoff radius of 6,500 m to bound the tessellation tiles. This distance was based on the maximum detection distance of individual Blainville’s beaked whale clicks at a U.S. Naval range in the Bahamas (Marques, Thomas, Ward, DiMarzio, and Tyack, 2009). Different combinations of hydrophones were recorded during different SCCs, so separate tessellations were created for each SCC.

2.2.2 M1: Modelling the pre-activity probability of dive detection

In the first model, we used data collected prior to SCCs, when no naval ships were present on the range and no other naval activity was known to occur, to model the spatial distribution of GVP detections across the range. Because of the way that GVPs were assigned to hydrophones (see Section 2.1.1) the data were not continuous in space. To account for this, we used a Markov random field (MRF) implemented in the R package `mgcv` (Wood, 2017) to model the spatial distribution of GVP detections. Markov random fields (Rue and Held, 2005) model correlation in space between discrete spatial units (henceforth, “tiles”). The correlation between two tiles is dictated by distance, as measured by the number of other tiles one needs pass through to travel between two tiles (“hops”); correlation is strongest between a tile and its direct neighbors (those tiles it shares a border with) and decreases with additional hops. This was appropriate for our data as we did not know where in each tile a given GVP occurred, but we assumed that it did occur in that tile.

We modelled the probability of a GVP at tile i as a Bernoulli trial: $\text{GVP}_i \sim \text{Bin}(1, \mu_{\text{M1},i})$. The linear predictor for on the logit scale was given as:

$$\text{logit}(\mu_{\text{M1},i}) = \beta_{\text{M1},0} + f(\text{MRF}_{i,s}) + f(\text{Depth}_i) + \log_e A_i, \quad (\text{M1})$$

where $\beta_{M1,0}$ is an intercept, $f(\text{MRF}_{i,s})$ denotes the Markov random field used to smooth space in SCC s , $f(\text{Depth}_i)$ is a smooth of depth (using a thin plate spline; Wood (2003)) and $\log_e A_i$ is an offset for the area (in km^2) of each tile, A_i . The offset term accounts for changes in probabilities of GVP detection due to the different areas monitored by each hydrophone. Because the hydrophone tessellation changed between SCCs (as there were different sets of hydrophones recorded during each SSC), separate MRFs were used for each SCC, but a single smoothing parameter was estimated across all MRFs. This allowed for different spatial smooths for each SCC, but constrained the smooths to have the same amount of wiggleness. The smooth of depth was shared across SCCs. We used this model to predict the baseline probability of a GVP detection at each hydrophone.

2.2.3 M2: Modelling the effect of Naval activity

For the second model, we used data collected for a few days prior to the onset of hull-mounted MFAS used during SCCs, when other naval training activities occurred at PMRF. Various vessels were present on the range during this period and other noise sources, including torpedoes and submarines, may have been present. We used data collected when training activity was present on the range, but hull-mounted MFAS was not used, to model the effect of general naval activity on beaked whale GVPs. Initially, we tried to use low-frequency noise levels in the 10-999 Hz range measured on range hydrophones as a covariate in this model, but found that the measured noise levels were not consistent with known locations of naval training activities.

We used the predicted baseline probability of a GVP detection from M1 as an offset to control for the underlying spatial distribution of GVPs. The model for the data when ships were present was intercept-only, with an offset derived from M1. We again modelled GVP presence at tile i as $\text{GVP}_i \sim \text{Bin}(1, \mu_{M2,i})$, with a linear predictor on the logit scale:

$$\text{logit}(\mu_{\mathbf{M2},i}) = \beta_{\mathbf{M2},0} + \log_e \xi_{\mathbf{M1},i}, \quad (\mathbf{M2})$$

where $\beta_{\mathbf{M2},0}$ is an intercept and $\xi_{\mathbf{M1},i}$ is the prediction (on the logit scale) for tile i using model **M1**, included as an offset term.

2.2.4 **M3: Modelling the effect of hull-mounted MFAS**

For the third model, we used data collected when hull-mounted MFAS was present on the range to model the effect of sonar on beaked whales. The probability of a GVP when sonar was present was modeled as a function of the maximum received level (modeled at each hydrophone for each half-hour period; see section 2.2). We assumed that as the maximum received level increased, the probability of dives decreased and modeled this using a monotonically decreasing smooth implemented in the R package **scam** (Pya and Wood, 2015). To ensure that the model predictions were the same at a maximum received level of 0 dB and when ships were not present, we did not include an intercept. GVP presence at tile i was modelled as a Bernoulli trial $\mathbf{GVP}_i \sim \text{Bin}(1, \mu_{\mathbf{M3},i})$ where the linear predictor on the logit scale was:

$$\text{logit}(\mu_{\mathbf{M3},i}) = f(\mathbf{MaxRL}_i) + \log_e \xi_{\mathbf{M2},i}, \quad (\mathbf{M3})$$

where $f(\mathbf{MaxRL}_i)$ was modeled as a monotonic decreasing smooth, $\xi_{\mathbf{M2},i}$ denotes the prediction (on the logit scale) for tile i when naval training activities were present on the range using model **M2**.

2.2.5 Uncertainty propagation

We used posterior simulation (sometimes referred to as a parametric bootstrap; Wood, Li, Shaddick, and Augustin, 2017) to propagate uncertainty through M1, M2, and M3. This consisted of sampling from the posterior distribution of the parameters for each model in turn, calculating predictions using these parameters and then refitting the subsequent model with updated offsets. Following this procedure through from M1 to M2 to M3 incorporated uncertainty from each model in the final predictions of the probability of detecting a GVP given different combinations of covariates.

The prediction grid contained all possible combinations of covariates within the realized covariate space; i.e., each hydrophone for each SCC with associated location, hydrophone depth, and area of the tessellation tile, presence/absence of naval activity, and, if naval activity was present, then either sonar absence or sonar received level between 100 and 190 dB in intervals of 5 dB.

Based on the resulting final posterior distribution of results (for model M3) we used appropriate quantiles to obtain average predictions and intervals. Mathematical details of the procedure are given in Appendix S1.

2.2.6 Quantifying the change in probability of GVPs

Finally, we calculated the expected change in the probability of detecting a GVP at each hydrophone $\mathbb{P}(\text{GVP})$ relative to either the probability of detecting a GVP when no general naval training activity was present and no MFAS was present ($\Delta_{M3':M1'}$), or relative to probability of detecting a GVP when general naval training activity was present but no MFAS was present ($\Delta_{M3':M2'}$).

Using the N_b posterior samples, we calculated the expected $\mathbb{P}(\text{GVP})$ under each set of covariates as

$$\mathbb{P}(\text{GVP}) = \text{logit}^{-1}(\mu_{\mathbf{M}'}), \quad (1)$$

for each $\mathbf{M}' = \mathbf{M1}', \mathbf{M2}'$, and $\mathbf{M3}'$. Then, we calculated the change in $\mathbb{P}(\text{GVP})$ for each set of covariates between $\mathbf{M3}'$ and $\mathbf{M1}'$ ($\Delta_{\mathbf{M3}':\mathbf{M1}'}$) and between $\mathbf{M3}'$ and $\mathbf{M2}'$ ($\Delta_{\mathbf{M3}':\mathbf{M2}'}$) for each realization of the posterior simulation.

$$\Delta_{\mathbf{M3}':\mathbf{M1}'} = \frac{\mathbb{P}(\text{GVP})_{\mathbf{M3}'} - \mathbb{P}(\text{GVP})_{\mathbf{M1}'}}{\mathbb{P}(\text{GVP})_{\mathbf{M1}'}} \quad (2)$$

$$\Delta_{\mathbf{M3}':\mathbf{M2}'} = \frac{\mathbb{P}(\text{GVP})_{\mathbf{M3}'} - \mathbb{P}(\text{GVP})_{\mathbf{M2}'}}{\mathbb{P}(\text{GVP})_{\mathbf{M2}'}} \quad (3)$$

For each received level we calculated the 2.5th, 50th, and 97.5th quantiles of $\Delta_{\mathbf{M3}':\mathbf{M1}'}$ and $\Delta_{\mathbf{M3}':\mathbf{M2}'}$ to create 95% CIs of change in $\mathbb{P}(\text{GVP})$ across possible received levels. We consider that the probability of disturbance is equal to 1 wherever the 95% CI does not include 0, and 0 otherwise.

2.2.7 Implementation

Code and data are available at [CITE zenodo repo].

3 Results

3.1 Results of Data Collection and Processing

Data were collected before and during six SCCs: two each in 2013, 2014, and 2017 (Table 1). The number of hydrophones for which recordings were available for each SCC varied from 49 to 61. A total of 190,928 30-min observations were made.

Table 1: Number of hydrophones used and number of observations made (no. 30-min periods) for each SCC before the exercise began, when naval activity was present, and when Naval activity and MFAS were present.

SCC	HPs	Pre-Activity	Nav. Activity	MFA Sonar
Feb13	61	114	193	124
Aug13	61	209	115	97
Feb14	60	513	111	129
Aug14	61	263	120	128
Feb17	59	450	97	108
Aug17	49	270	106	113

The exact timing of activities during these exercises varied (Fig. 2). For most SCCs, pre-activity data were available immediately preceding the onset of Naval training activity; however, in February 2013 the only available pre-activity data were collected almost a month prior to the onset of Naval training activity. In some SCCs, weekends or other breaks in training resulted in a break in training activity on the range during the days preceding MFAS use. MFAS was used for 3-4 days during each training event.

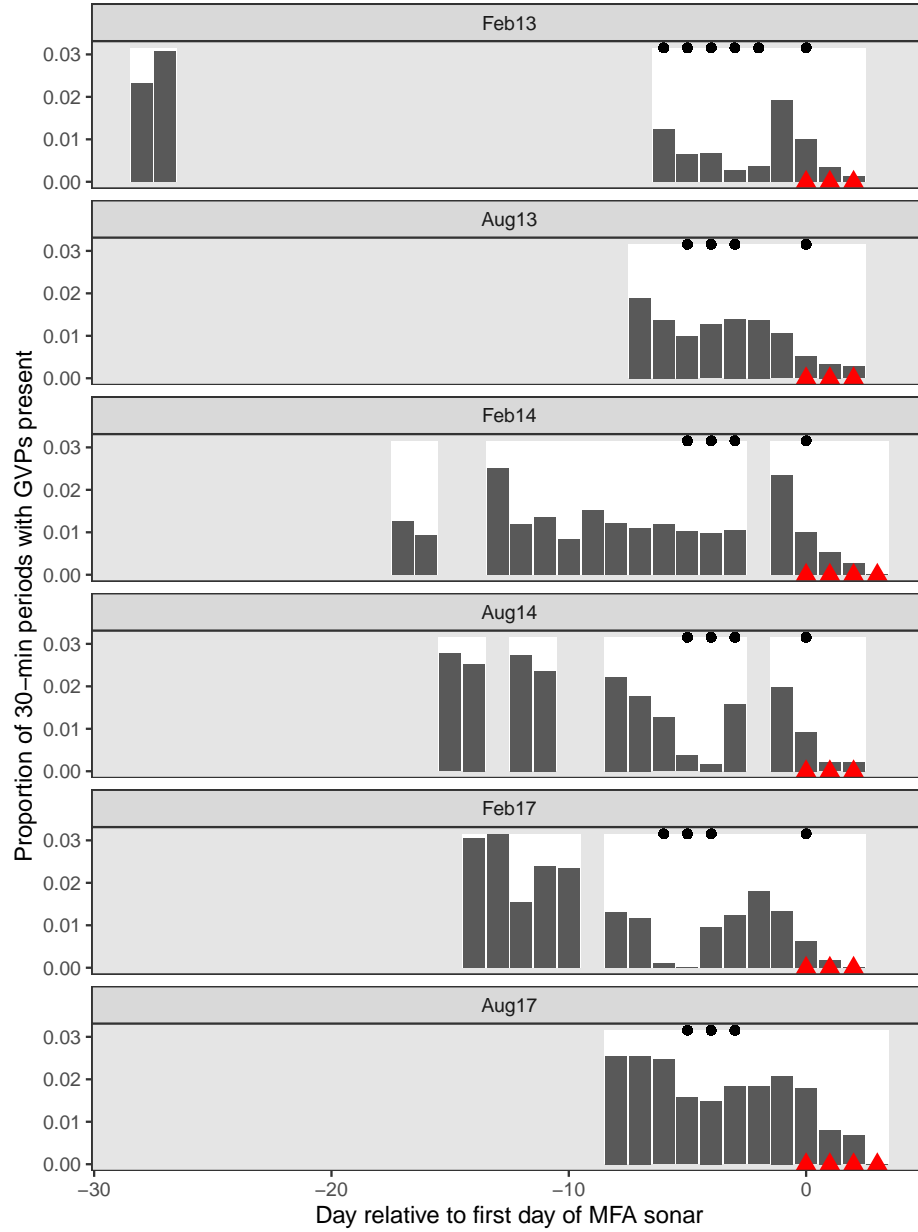


Figure 2: Timeseries of six recorded Naval training activities at PMRF. The timeseries are aligned relative to the first day that MFAS (red triangles) was used in each exercise (horizontal axis). Days with white background indicate days for which recordings and data were available. Dark gray bars indicate the proportion of 30-min periods on each day, across all hydrophones, when GVPs were detected (vertical axis). Black dots indicate days when Naval activity was present on the range.

Across all SCCs, hydrophones, and conditions, a total of 2,312 GVPs were identified. The average probability of detecting a GVP was therefore 1%. The spatial distribution of GVPs differed during the pre-activity phases of SCCs (Fig. S2.3; top panel).

Modelled maximum received levels ranged from 38 to 186 dB re. 1μ Pa, with a median value when MFAS was present of 147 dB re. 1μ Pa. The intensity and spatial distribution of MFAS received levels varied across the range and across SCCs (Fig. S2.4).

Based on the observed data, the probability of detecting a GVP changed by -57% when general naval training activity was present compared to when naval activity was absent, by -47% when naval activity and MFAS were present compared to when only naval activity was present, and by -77% when naval activity and MFAS were present compared to when neither naval activity nor sonar were present (Fig. S2.2).

3.2 Results of spatial modelling

We created separate tessellations for each SCC (Fig. S2.1). In August 2017, data were available from fewer hydrophones, and so in some cases the tessellated tiles, with bounding radius of 6,500 m, did not completely cover the range. Hydrophone depths varied from 648 to 4716 m.

M1 fitted a spatial model of $\mathbb{P}(\text{GVP})$ to data collected prior to the onset of naval training activity. This model used a MRF smooth to account for the spatial structure of the range and a spline on depth, with an offset for the log of the area effectively monitored by each hydrophone. Both the MRF and spline on depth were significant at the $\alpha = 0.05$ level (p -value $< 2\text{E-}16$). The model explained 14.1% of deviance in the dataset, and visual inspection of observed versus predicted values indicated a good fit to the data (Fig. S3.X). The model **M1** predicted highest $\mathbb{P}(\text{GVP})$ at hydrophone depths between 1,500 and 2,000 m (Fig. S3.X).

M2 used the predicted values from **M1** as an offset and fitted a model of to data when naval

activity was ongoing, as indicated by the presence of naval ships on the range. This model was intercept-only, and $\mathbb{P}(\text{GVP})$ when naval activity was ongoing was significantly different from the baseline period at the $\alpha = 0.05$ level ($p\text{-value} < 2\text{E-}16$). The expected $\mathbb{P}(\text{GVP})$ decreased by a median of 64% (95% CI 59% - 68%) when naval activity was present compared to when it was absent.

M3 used the predicted values from M2 as an offset and fitted a model to data when naval activity and MFAS were present. This model used a monotonically decreasing spline on modelled MFAS received level (Fig. SX) and did not include an intercept term. The smooth on MFAS received level was significant at the $\alpha = 0.05$ level ($p\text{-value} = 6.74\text{E-}10$) and the model explained 12.4% of deviance in the data.

For MFAS received levels above 100 dB re. 1 μPa , change in $\mathbb{P}(\text{GVP})$ was calculated relative to the pre-activity baseline period ($\Delta_{M3':M1'}$) and to the period when naval activity was present on the range ($\Delta_{M3':M2'}$; Fig. 4 & Fig. 5). At a received level of 150 dB, $\Delta_{M3':M1'}$ was -92% (95% CI -100% - -87%) and $\Delta_{M3':M2'}$ was -78% (95% CI -100% - -62%). Relative to when only naval training is present, $\Delta_{M3':M2'}$ predicts a 50% reduction in $\mathbb{P}(\text{GVP})$ at a MFAS received level of 135 dB re 1 μPa .

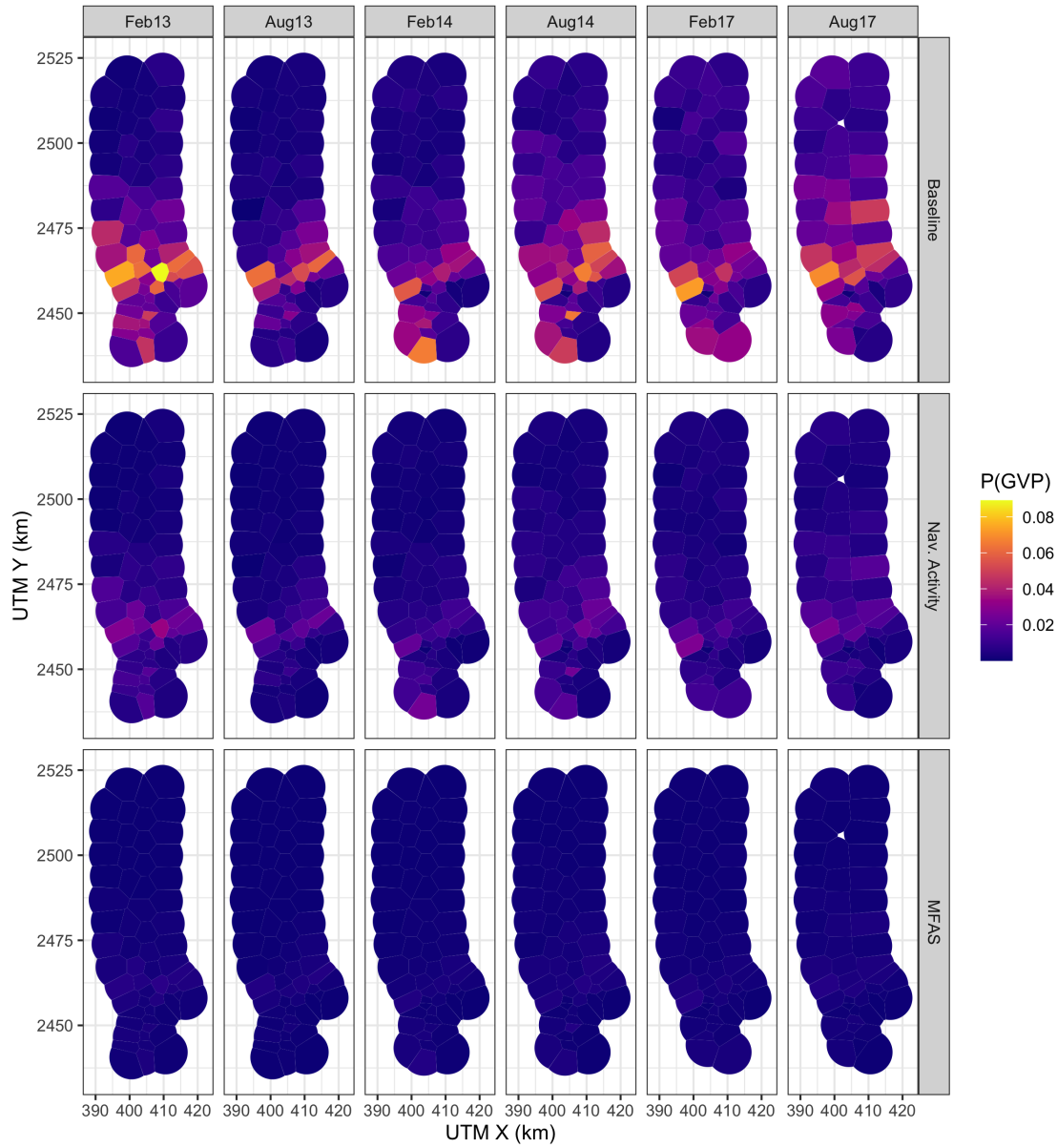


Figure 3: Map of expected probability of detecting a GVP (color scale) at each hydrophone during each SCC (columns) prior to the onset of naval training activity, during naval training activity when no MFAS was present, and during naval training activity when MFAS was present at a level of 150 dB re. 1 μ Pa rms (rows).

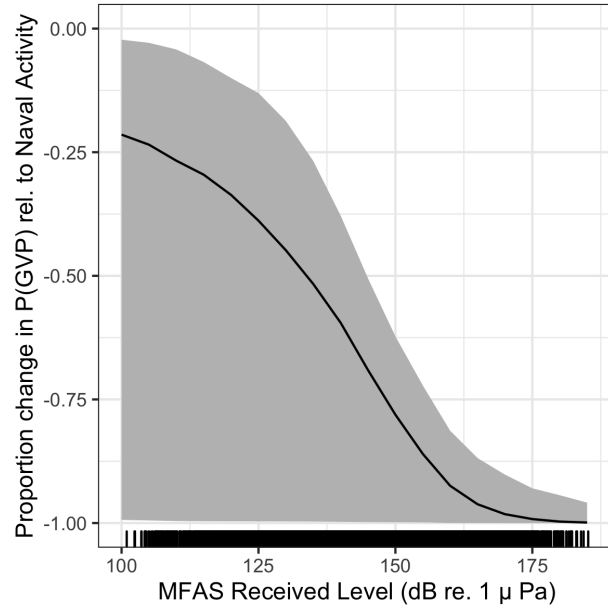


Figure 4: Median (black line) and 95% CIs (gray shading) expected change in the probability of detecting a group vocal period (vertical axis) with increasing MFAS received level (horizontal axis) relative to when naval training activity but no MFAS is present on the range.

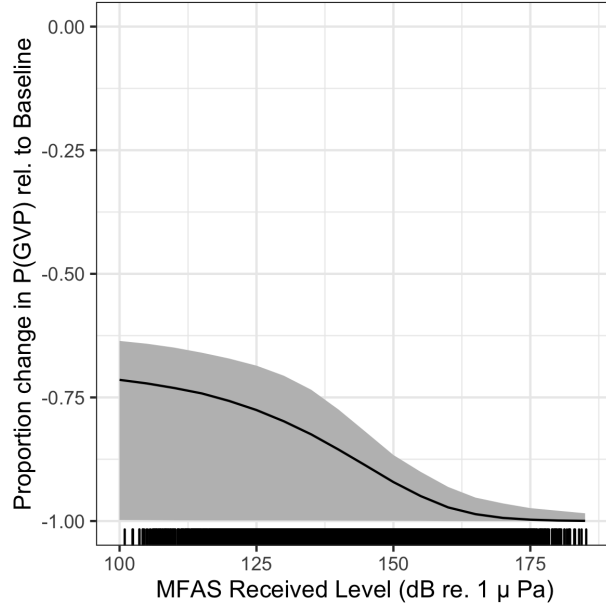


Figure 5: Median (black line) and 95% CIs (gray shading) expected change in the probability of detecting a group vocal period (vertical axis) with increasing MFAS received level (horizontal axis) relative to when neither naval training activity nor MFAS is present on the range.

4 Discussion

We used a series of three linked models to quantify the response of Blainville’s beaked whales to naval training exercises involving MFAS: the first model was fitted to pre-exercise baseline data, the second was fitted to data collected when naval training exercises were ongoing but no MFAS was present, and the third model was fitted to data collected during naval training exercises that used MFAS. We found that the probability of acoustic detections of Blainville’s beaked whales decreased when both naval training exercises and naval training exercises using MFAS were present (Fig. 4 and 5).

The methods presented here are spatially-explicit and account for the spatial confounding of animal distribution and naval training activity. The data used in this study are from an undesigned experiment, where the spatial intensity of the treatments (naval activity and

MFAS) were not applied randomly with respect to either the study area or Blainville’s beaked whale presence. We did not want the spatial distribution of training exercises and MFAS to influence our understanding of the baseline spatial distribution of Blainville’s beaked whales. Due to the spatial confounding of animal distribution and naval training activity at PMRF, fitting a single model to all of the data would lead to underestimating the impact of sonar, since changes in distribution due to MFAS could be explained as spatial changes by the MRF (Appendix S3). Our three-stage modelling approach addresses this issue while propagating uncertainty between the models. This is a novel application of GAMs.

The analytical approach outlined in this article could be applied to other species, regions, and types of disturbance where experimental design is not possible. The use of Markov random fields for the spatial term is useful for cases where exact distance data is not available, avoiding the use of continuous smoothers when true location data is not available. Shape-constrained smoothing is also well-suited to the kind of data we modelled here – ensuring that values can only stay constant or decrease over time (or any other covariate). Finally, the use of a multi-stage posterior sampling scheme extends to any situation where multiple models are fitted and the results of one part feed into another. Simulation-based approaches such as these bypass the need to derive (often complex) expressions (or shortcut them by assuming independence).

In a regulatory context, a dose-response function as presented in Figs. 4 and 5 is often interpreted as representing the proportion of a population that responds (vertical axis) to a given received level (horizontal axis) (Tyack and Thomas, 2019). However, the metric used in this study – the change in the probability of detecting a GVP within a 30-min period – does not directly correspond to the proportion of the population that is affected. Rather, it may reflect a change in the proportion of time that all individuals in the population spent foraging. These two interpretations have different implications for understanding sub-lethal impacts of MFAS. In the traditional interpretation, given exposure to a certain received level,

some of the population is affected and some of the population is not. In our interpretation, the entire exposed population is affected.

In comparison to the risk function developed by Moretti et al. (2014) for Blainville's beaked whales at AUTECH, our risk function predicts a more intense response to naval sonar. This may be because Moretti et al. were not able to explicitly account for the effects of naval training activities that did not include MFAS. Their baseline period consisted of 19 hours of data before the onset of MFAS; as at PMRF, it is likely that training activities during this period included sound sources other than MFAS. Therefore, their risk function is probably more analogous to our expected change in the probability of a detection when MFAS is present relative to when naval training activity was present (Fig. 4). In the future, we would like to further investigate the specific causes of changes in the probability of detecting GVPs before the onset of MFAS. The reduction in detection of foraging dives could be a response to general Naval training activity on the range, or to specific sound sources that have not previously been studied. Alternatively, it is possible that Blainville's beaked whales are semi-resident on the range and have become habituated to SCC activity; they may move off the range in anticipation of MFAS.

The findings presented here and in Moretti et al. (2014) may be applicable to other species and regions, though species-specific dive behaviors and regional differences in oceanography likely modulate the impact of MFAS. The AUTECH range is located in a deep basin bounded to the south, east, and west by shallow waters and with maximum depths of 2,000 m. In contrast, the PMRF occurs across a steep slope and into deep water, over 5,000 m in depth. Although the environments at PMRF and AUTECH are different, the foraging dive behavior of Blainville's beaked whales is similar at AUTECH and PMRF; dives occur in deeper waters over steep slopes with gradients ranging from 3-23%, although dives occur in deeper waters (2,000-3,000 m; Henderson et al., 2016) at PMRF than at AUTECH (500-1,300 m; MacLeod and Zuur, 2005, Hazen, Nowacek, St. Laurent, Halpin, and Moretti (2011)). Resident Blainville's

beaked whales off the Big Island also occur in slightly shallower waters than at PMRF, from 980-1,410 m (R. W. Baird, 2011; R. W. Baird, Webster, Schorr, McSweeney, and Barlow, 2008). Therefore it is likely the location of the mesopelagic scattering layer along the slope that drives the location of Blainville’s beaked whales rather than the bathymetric depth; this is supported by the fact that dive depths are similar across areas, occurring on average down to 1,050-1,150 m for 46-60 min (R. W. Baird et al., 2008; Joyce et al., 2017; Schorr et al., 2009).

Similarly, documented responses to MFAS activity are comparable at both ranges, with individuals and groups moving to the periphery of the range or off the range and returning 2-4 days after the cessation of the sonar (Joyce et al., 2019; Manzano-Roth et al., 2016; McCarthy et al., 2011). Resident animals that are frequently exposed to training activity and transient animals that only encounter MFAS occasionally are likely to respond differently to sonar; it is not known how resident the Blainville’s beaked whales are at PMRF, and there may be offshore animals as well found on the northern hydrophones. Regardless, the similarities in Blainville’s beaked whale behavioral responses to Navy training activity across different ranges and environments and at similar received levels may indicate the intrinsic nature of the response. Conducting a similar analysis of Cuvier’s beaked whale responses at the Southern California Anti-Submarine Warfare Range (SOAR) would further support this assessment; existing findings already demonstrate that Cuvier’s respond in a similar manner by reducing their foraging dives and moving away from the ensonified area (DeRuiter et al., 2013; Falcone et al., 2017).

Acknowledgements

This study was funded by the US Navy Living Marine Resources Program (Contract No. N39430-17-P-1983).

414 **Authors' Contributions**

415 Conceptualization: E.E.H., D.J.M, L.T.

416 Data curation: E.K.J., E.E.H.

417 Formal analysis: E.K.J., E.E.H., C.S.O.

418 Funding acquisition: E.E.H., D.J.M., L.T.

419 Investigation: E.E.H.

420 Methodology: E.K.J., E.E.H., D.L.M., C.S.O., L.T.

421 Software: E.K.J., D.L.M., C.S.O. Supervision: L.T.

422 Visualization: E.K.J.

423 Writing – original draft: E.K.J., E.E.H., D.L.M.

424 Writing – review & editing: E.K.J, E.E.H., D.L.M., C.S.O., D.J.M., L.T.

425 **ORCID**

426 Eiren K. Jacobson: <https://orcid.org/0000-0003-0147-8367>

427 David L. Miller: <https://orcid.org/0000-0002-9640-6755>

428 Cornelia S. Oedekoven: <https://orcid.org/0000-0002-5610-7814>

429 Len Thomas: <https://orcid.org/0000-0002-7436-067X>

References

- Aguilar de Soto, N., Johnson, M., Madsen, P. T., Tyack, P. L., Bocconcelli, A., & Fabrizio Borsani, J. (2006). Does intense ship noise disrupt foraging in deep-diving Cuvier's beaked whales (*Ziphius cavirostris*)? *Marine Mammal Science*, 22(3), 690–699. <https://doi.org/10.1111/j.1748-7692.2006.00044.x>
- Aguilar de Soto, N., Madsen, P. T., Tyack, P., Arranz, P., Marrero, J., Fais, A., ... Johnson, M. (2012). No shallow talk: Cryptic strategy in the vocal communication of Blainville's beaked whales. *Marine Mammal Science*, 28(2), E75–E92. <https://doi.org/10.1111/j.1748-7692.2011.00495.x>
- Baird, R. W. (2011). Short Note: Open-Ocean Movements of a Satellite-Tagged Blainville's Beaked Whale (*Mesoplodon densirostris*): Evidence for an Offshore Population in Hawai'i? *Aquatic Mammals*, 37(4), 506–511. <https://doi.org/10.1578/AM.37.4.2011.506>
- Baird, R. W., Webster, D. L., Schorr, G. S., McSweeney, D. J., & Barlow, J. (2008). Diel variation in beaked whale diving behavior. *Marine Mammal Science*, 24(3), 630–642. <https://doi.org/10.1111/j.1748-7692.2008.00211.x>
- Bernaldo de Quirós, Y., Fernandez, A., Baird, R. W., Brownell, R. L., Aguilar de Soto, N., Allen, D., ... Schorr, G. (2019). Advances in research on the impacts of anti-submarine sonar on beaked whales. *Proceedings of the Royal Society B: Biological Sciences*, 286(1895), 20182533. <https://doi.org/10.1098/rspb.2018.2533>
- Cox, T., Ragen, T., Read, A., Vos, E., Baird, R., Balcomb, K., ... others. (2006). Understanding the impacts of anthropogenic sound on beaked whales1. *Journal of Cetacean Research and Management*, 7(3), 177–187.
- DeRuiter, S. L., Southall, B. L., Calambokidis, J., Zimmer, W. M. X., Sadykova, D., Falcone, E. A., ... Tyack, P. L. (2013). First direct measurements of behavioural responses by

Cuvier's beaked whales to mid-frequency active sonar. *Biology Letters*, 9(4), 20130223.
<https://doi.org/10.1098/rsbl.2013.0223>

Falcone, E. A., Schorr, G. S., Watwood, S. L., DeRuiter, S. L., Zerbini, A. N., Andrews, R. D., . . . Moretti, D. J. (2017). Diving behaviour of Cuvier's beaked whales exposed to two types of military sonar. *Royal Society Open Science*, 4(8), 170629. <https://doi.org/10.1098/rsos.170629>

Harris, C. M., Martin, S. W., Martin, C., Helble, T. A., Henderson, E. E., Paxton, C. G. M., & Thomas, L. (2019). Changes in the Spatial Distribution of Acoustically Derived Minke Whale (*Balaenoptera acutorostrata*) Tracks in Response to Navy Training. *Aquatic Mammals*, 45(6), 661–674. <https://doi.org/10.1578/AM.45.6.2019.661>

Hazen, E. L., Nowacek, D. P., St. Laurent, L., Halpin, P. N., & Moretti, D. J. (2011). The Relationship among Oceanography, Prey Fields, and Beaked Whale Foraging Habitat in the Tongue of the Ocean. *PLoS ONE*, 6(4), e19269. <https://doi.org/10.1371/journal.pone.0019269>

Heaney, K. D., & Campbell, R. L. (2016). Three-dimensional parabolic equation modeling of mesoscale eddy deflection. *The Journal of the Acoustical Society of America*, 139(2), 918–926. <https://doi.org/10.1121/1.4942112>

Henderson, E. E., Martin, S. W., Manzano-Roth, R., & Matsuyama, B. M. (2016). Occurrence and Habitat Use of Foraging Blainville's Beaked Whales (*Mesoplodon densirostris*) on a U.S. Navy Range in Hawaii. *Aquatic Mammals*, 42(4), 549–562. <https://doi.org/10.1578/AM.42.4.2016.549>

Johnson, M., Madsen, P. T., Zimmer, W. M. X., Aguilar de Soto, N., & Tyack, P. L. (2004). Beaked whales echolocate on prey. *Proceedings of the Royal Society of London. Series B: Biological Sciences*, 271, S383–S386. <https://doi.org/10.1098/rsbl.2004.0208>

Johnson, M., Madsen, P. T., Zimmer, W. M. X., Soto, N. A. de, & Tyack, P. L. (2006).

Foraging Blainville’s beaked whales (*Mesoplodon densirostris*) produce distinct click types matched to different phases of echolocation. *Journal of Experimental Biology*, 209(24), 5038–5050. <https://doi.org/10.1242/jeb.02596>

Joyce, T. W., Durban, J. W., Claridge, D. E., Dunn, C. A., Fearnbach, H., Parsons, K. M., ... Ballance, L. T. (2017). Physiological, morphological, and ecological tradeoffs influence vertical habitat use of deep-diving toothed-whales in the Bahamas. *PLOS ONE*, 12(10), e0185113. <https://doi.org/10.1371/journal.pone.0185113>

Joyce, T. W., Durban, J. W., Claridge, D. E., Dunn, C. A., Hickmott, L. S., Fearnbach, H., ... Moretti, D. (2019). Behavioral responses of satellite tracked Blainville’s beaked whales (*Mesoplodon densirostris*) to mid-frequency active sonar. *Marine Mammal Science*, mms.12624. <https://doi.org/10.1111/mms.12624>

Macleod, C. D., & D’Amico, A. (2006). *A review of beaked whale behaviour and ecology in relation to assessing and mitigating impacts of anthropogenic noise*. 11.

MacLeod, C. D., & Zuur, A. F. (2005). Habitat utilization by Blainville’s beaked whales off Great Abaco, northern Bahamas, in relation to seabed topography. *Marine Biology*, 147(1), 1–11. <https://doi.org/10.1007/s00227-004-1546-9>

Madsen, P. T., Aguilar de Soto, N., Arranz, P., & Johnson, M. (2013). Echolocation in Blainville’s beaked whales (*Mesoplodon densirostris*). *Journal of Comparative Physiology A*, 199(6), 451–469. <https://doi.org/10.1007/s00359-013-0824-8>

Manzano-Roth, R., Henderson, E. E., Martin, S. W., Martin, C., & Matsuyama, B. (2016). Impacts of U.S. Navy Training Events on Blainville’s Beaked Whale (*Mesoplodon densirostris*) Foraging Dives in Hawaiian Waters. *Aquatic Mammals*, 42(4), 507–518. <https://doi.org/10.1578/AM.42.4.2016.507>

Marques, T. A., Thomas, L., Ward, J., DiMarzio, N., & Tyack, P. L. (2009). Estimating cetacean population density using fixed passive acoustic sensors: An example with

Blainville's beaked whales. *The Journal of the Acoustical Society of America*, 125(4), 1982–1994. <https://doi.org/10.1121/1.3089590>

Martin, C. R., Henderson, E. E., Martin, S. W., Helble, T. A., Manzano-Roth, R. A., Matsuyama, B. M., & Alongi, G. A. (2020). *FY18 Annual Report on Pacific Missile Range Facility Marine Mammal Monitoring*. Retrieved from Naval Information Warfare Center Pacific San Diego United States website: <https://apps.dtic.mil/sti/citations/AD1091141>

MATLAB. (2017). Natick, Massachusetts: The MathWorks Inc.

McCarthy, E., Moretti, D., Thomas, L., DiMarzio, N., Morrissey, R., Jarvis, S., . . . Dilley, A. (2011). Changes in spatial and temporal distribution and vocal behavior of Blainville's beaked whales (*Mesoplodon densirostris*) during multiship exercises with mid-frequency sonar. *Marine Mammal Science*, 27(3), E206–E226. <https://doi.org/10.1111/j.1748-7692.2010.00457.x>

Moretti, D., Thomas, L., Marques, T. A., Harwood, J., Dilley, A., Neales, B., . . . Morrissey, R. (2014). A Risk Function for Behavioral Disruption of Blainville's Beaked Whales (*Mesoplodon densirostris*) from Mid-Frequency Active Sonar. *PLoS ONE*, 9(1), e85064. <https://doi.org/10.1371/journal.pone.0085064>

New, L., Moretti, D. J., Hooker, S. K., Costa, D. P., & Simmons, S. E. (2013). Using Energetic Models to Investigate the Survival and Reproduction of Beaked Whales (family Ziphiidae). *PLoS ONE*, 8(7), e68725. <https://doi.org/10.1371/journal.pone.0068725>

Pirotta, E., Milor, R., Quick, N., Moretti, D., Di Marzio, N., Tyack, P., . . . Hastie, G. (2012). Vessel Noise Affects Beaked Whale Behavior: Results of a Dedicated Acoustic Response Study. *PLoS ONE*, 7(8), e42535. <https://doi.org/10.1371/journal.pone.0042535>

Pya, N., & Wood, S. N. (2015). Shape constrained additive models. *Statistics and Computing*,

25(3), 543–559. <https://doi.org/10.1007/s11222-013-9448-7>

R Core Team. (2018). *R: A Language and Environment for Statistical Computing*. Retrieved from <https://www.R-project.org/>

Rue, H., & Held, L. (2005). *Gaussian Markov Random Fields: Theory and Applications*. London: Chapman & Hall.

Schorr, Baird, Hanson, Webster, McSweeney, & Andrews, R. (2009). Movements of satellite-tagged Blainville’s beaked whales off the island of Hawai’i. *Endangered Species Research*, 10, 203–213. <https://doi.org/10.3354/esr00229>

Turner, R. (2019). *Deldir: Delaunay Triangulation and Dirichlet (Voronoi) Tessellation*. Retrieved from <https://CRAN.R-project.org/package=deldir>

Tyack, P. L., & Thomas, L. (2019). Using dose–response functions to improve calculations of the impact of anthropogenic noise. *Aquatic Conservation: Marine and Freshwater Ecosystems*, 29(S1), 242–253. <https://doi.org/10.1002/aqc.3149>

Tyack, P. L., Zimmer, W. M. X., Moretti, D., Southall, B. L., Claridge, D. E., Durban, J. W., . . . Boyd, I. L. (2011). Beaked Whales Respond to Simulated and Actual Navy Sonar. *PLoS ONE*, 6(3), e17009. <https://doi.org/10.1371/journal.pone.0017009>

U.S. Department of the Navy. (2017). Criteria and thresholds for US navy acoustic and explosive effects analysis (phase III). *Space and Naval Warfare Systems Command, US Navy, Department of Defence, San Diego, California*.

U.S. Department of the Navy. (2018). *Final Environmental Impact Statement/Overseas Environmental Impact Statement Hawaii-Southern California Training and Testing*. Retrieved from https://www.hstteis.com/portals/hstteis/files/hstteis_p3/feis/section/HSTT_FEIS_3.07_Marine_Mammals_October_2018.pdf

Wood, S. N. (2003). Thin plate regression splines. *Journal of the Royal Statistical Society:*

551 *Series B (Statistical Methodology)*, 65(1), 95–114. <https://doi.org/10.1111/1467-9868>.

552 00374

553 Wood, S. N. (2017). *Generalized Additive Models: An Introduction with R* (2nd ed.).

554 Chapman; Hall/CRC.

555 Wood, S. N., Li, Z., Shaddick, G., & Augustin, N. H. (2017). Generalized Additive Models

556 for Gigadata: Modeling the U.K. Black Smoke Network Daily Data. *Journal of the*

557 *American Statistical Association*, 112(519), 1199–1210. <https://doi.org/10.1080/01621459>.

558 2016.1195744

S1: Uncertainty estimation details

We used posterior simulation to propagate uncertainty through M1, M2, and M3. Each model was fitted via restricted maximum likelihood (REML), so the resulting estimates were empirical Bayes estimates. In this case we generated samples from the (approximately multivariate normal) posterior of the model parameters. We generated a sample of the model parameters, $\beta^* \sim \text{MVN}(\hat{\beta}, \mathbf{V}_{\hat{\beta}})$, where $\hat{\beta}$ was the estimate of the model coefficients and $\mathbf{V}_{\hat{\beta}}$ was the posterior covariance matrix. We then used the matrix that maps the model parameters to the predictions on the linear predictor scale (\mathbf{X}_p ; Wood et al. 2017; section 7.2.6), along with the inverse link function to generate predictions for each posterior sample. Here the β for each model included the coefficients for the smooth terms in the model and fixed effects (e.g., intercept) if present. Predictions, μ^* , were written as:

$$\mu^* = g^{-1}(\eta^*) = g^{-1}(\mathbf{X}_p \beta^* + \xi),$$

where g was the link function, η^* was the linear predictor and ξ was any offset used by this prediction. By sampling from the posterior of β , and then taking the empirical variance of the resulting predictions, we obtained variance estimates (Wood et al. 2017; section 7.2.6). The prediction grid contained all possible combinations of covariates within the realized covariate space; i.e., each hydrophone for each SCC with associated location, hydrophone depth, and area of the tessellation tile, presence/absence of naval activity, and, if naval activity was present, then either sonar absence or sonar received level between 35 and 190 dB in intervals of 5 dB. This procedure was repeated for each model, with refitting to updated offsets from the previous model.

An algorithm for calculating the variance from our multi-stage approach is as follows. First define N_b as the number of samples to make, let $\mathbf{X}_{p,Mj}$ for $j = 1, 2, 3$ be the matrix that maps coefficients to the predictions for model Mj. For N_b times:

- 582 1. Draw a sample from the posterior of M1: $\tilde{\beta}_{\mathbf{M1}} \sim \text{MVN}(\hat{\beta}_{\mathbf{M1}}, \mathbf{V}_{\mathbf{M1}})$.
- 583 2. Calculate a new offset for M2, $\tilde{\xi}_{\mathbf{M1}} = \mathbf{X}_{p,\mathbf{M1}}\tilde{\beta}_{\mathbf{M1}} + \log_e \mathbf{A}$.
- 584 3. Refit M2 with $\tilde{\xi}_{\mathbf{M1}}$ as the offset, to obtain M2'.
- 585 4. Draw a sample from the posterior of M2': $\tilde{\beta}_{\mathbf{M2}'} \sim \text{MVN}(\hat{\beta}_{\mathbf{M2}'}, \mathbf{V}_{\mathbf{M2}'})$
- 586 5. Calculate a new offset for M3, $\tilde{\xi}_{\mathbf{M2}} = \mathbf{X}_{p,\mathbf{M2}}\tilde{\beta}_{\mathbf{M2}'} + \tilde{\xi}_{\mathbf{M1}}$ (predictions for the sonar data
587 locations for M2').
- 588 6. Refit M3 with offset $\tilde{\xi}_{\mathbf{M2}}$ to obtain M3'.
- 589 7. Predict $\mu_{\mathbf{M1}'}$, $\mu_{\mathbf{M2}'}$, and $\mu_{\mathbf{M3}'}$ over prediction grid and store them.

590 We then calculated summary statistics (means and variances) of the N_b values of $\mu_{\mathbf{M1}'}$, $\mu_{\mathbf{M2}'}$,
591 and $\mu_{\mathbf{M3}'}$ we generated. The empirical variance of the N_b values of $\mu_{\mathbf{M3}'}$ gave the uncertainty,
592 incorporating components from all three models. We took appropriate pointwise quantiles
593 to form confidence bands for the functional relationships between sonar received level and
594 estimated probability of detecting GVPs.

S2: Supplementary Tables and Figures

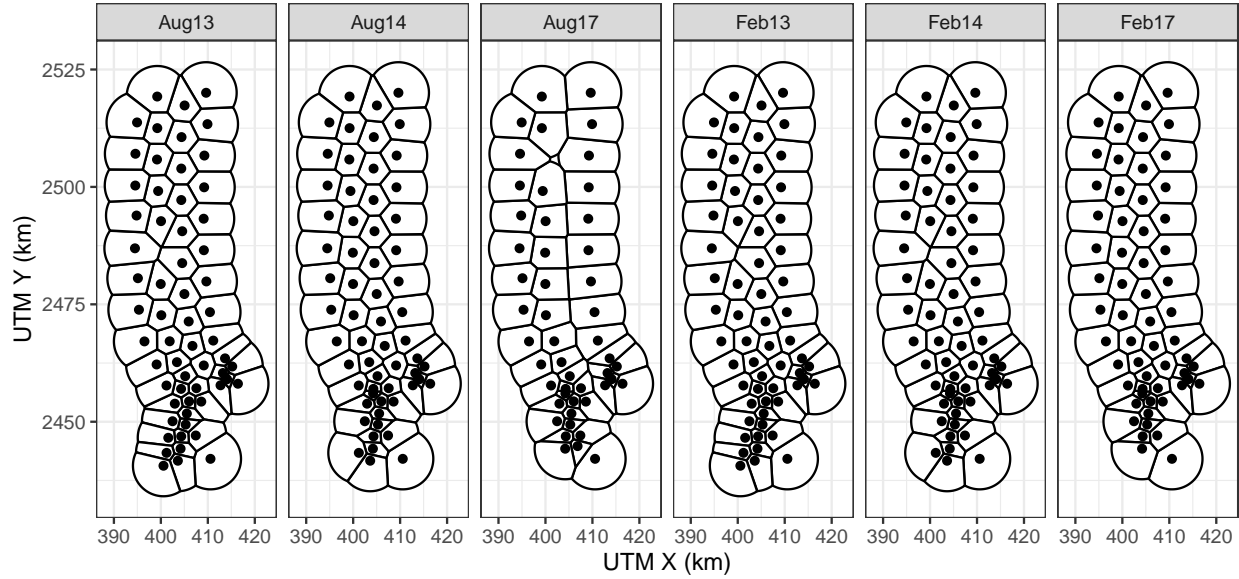


Figure S2.1: PMRF range tessellations for each of six recorded SCCs. Black lines indicate boundaries of hydrophone tiles. Black dots indicate approximate hydrophone locations.

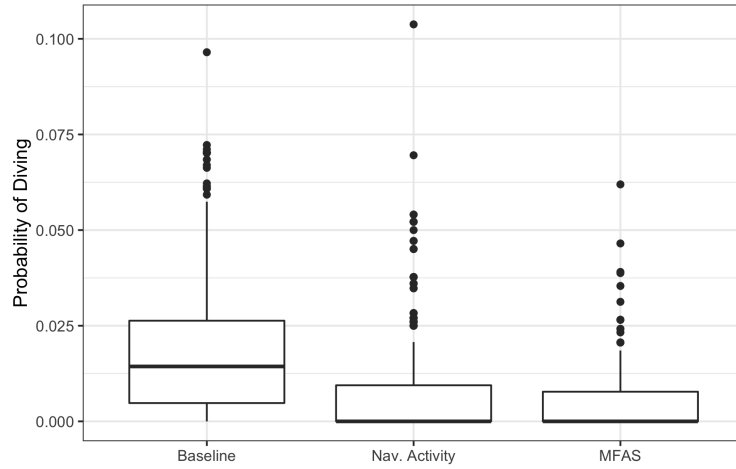


Figure S2.2: Boxplot of observed probability of a GVP across all hydrophones and SCCs (vertical axis) during baseline period, when naval activity was present, and when MFAS was present (horizontal axis).

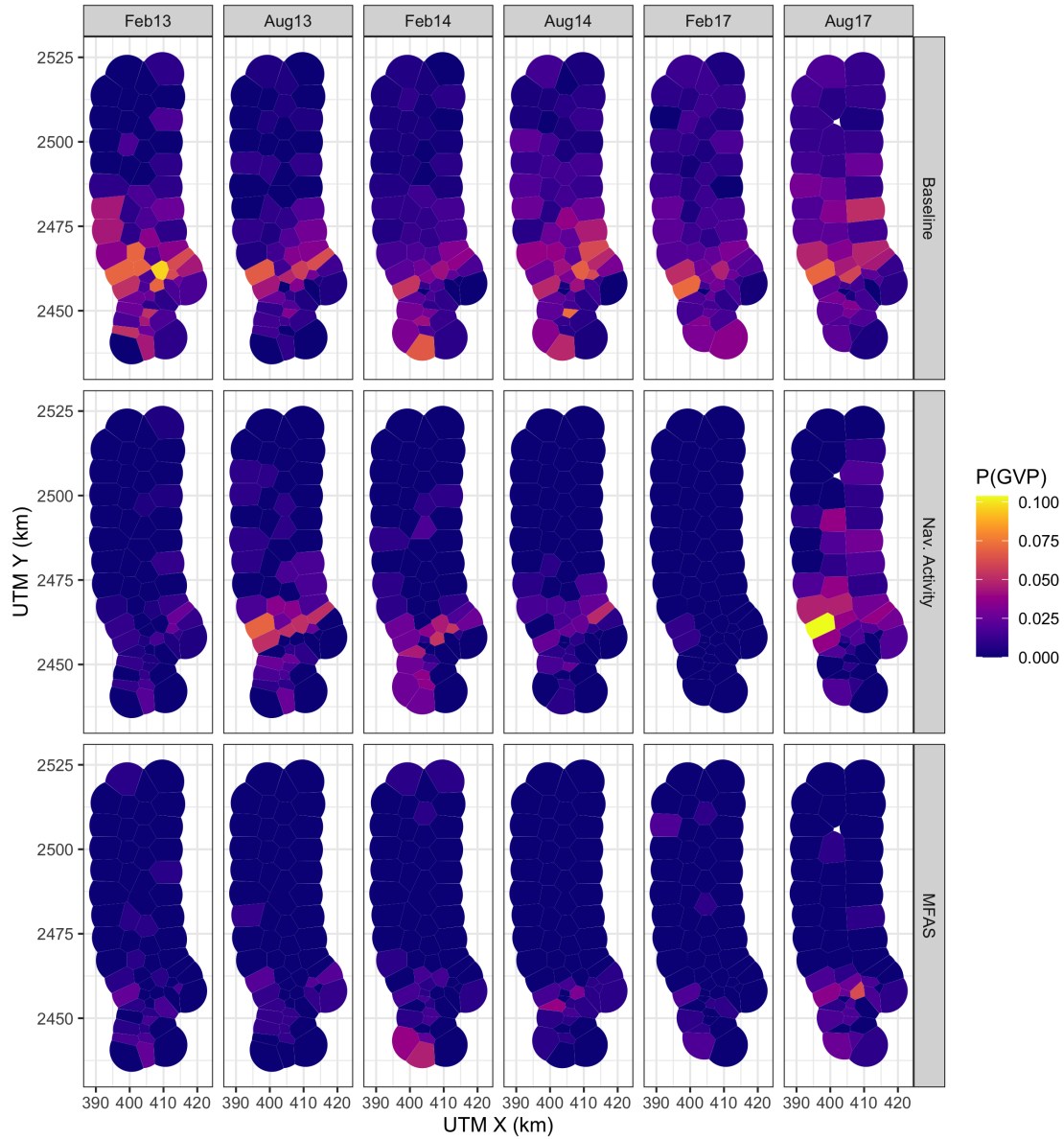


Figure S2.3: Map of observed probability of detecting a GVP at each hydrophone (color scale) during the baseline period, when naval activity was present, and when MFAS was present (rows) for each SCC (columns). Note that values of the probability of detecting a GVP are not corrected for effort (size of the hydrophone tile).

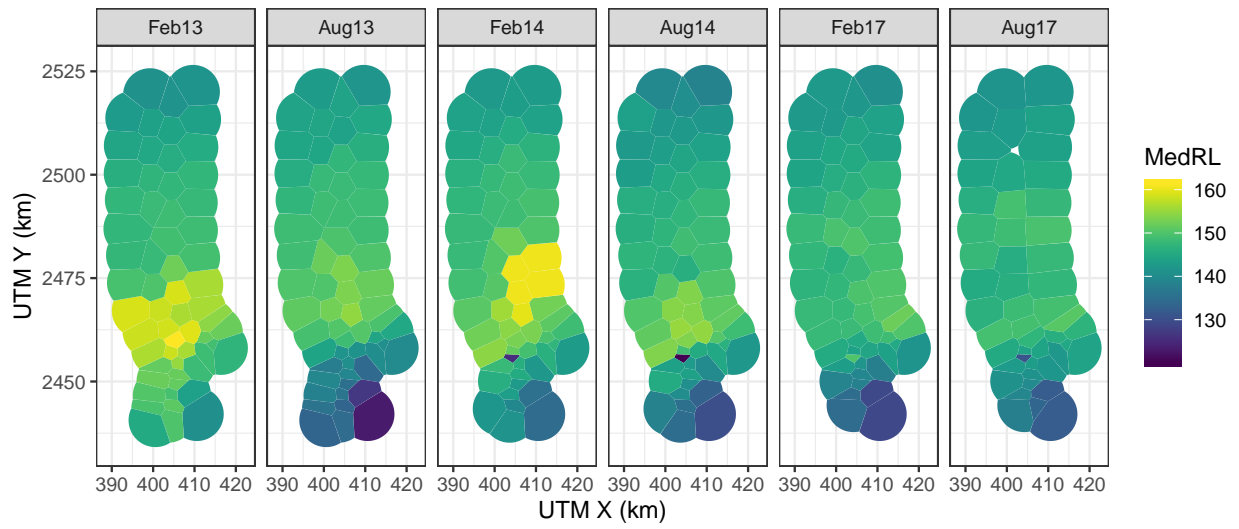


Figure S2.4: Median received level (dB re. 1 μ Pa) when MFAS was present (color scale) for all hydrophones and SCCs.

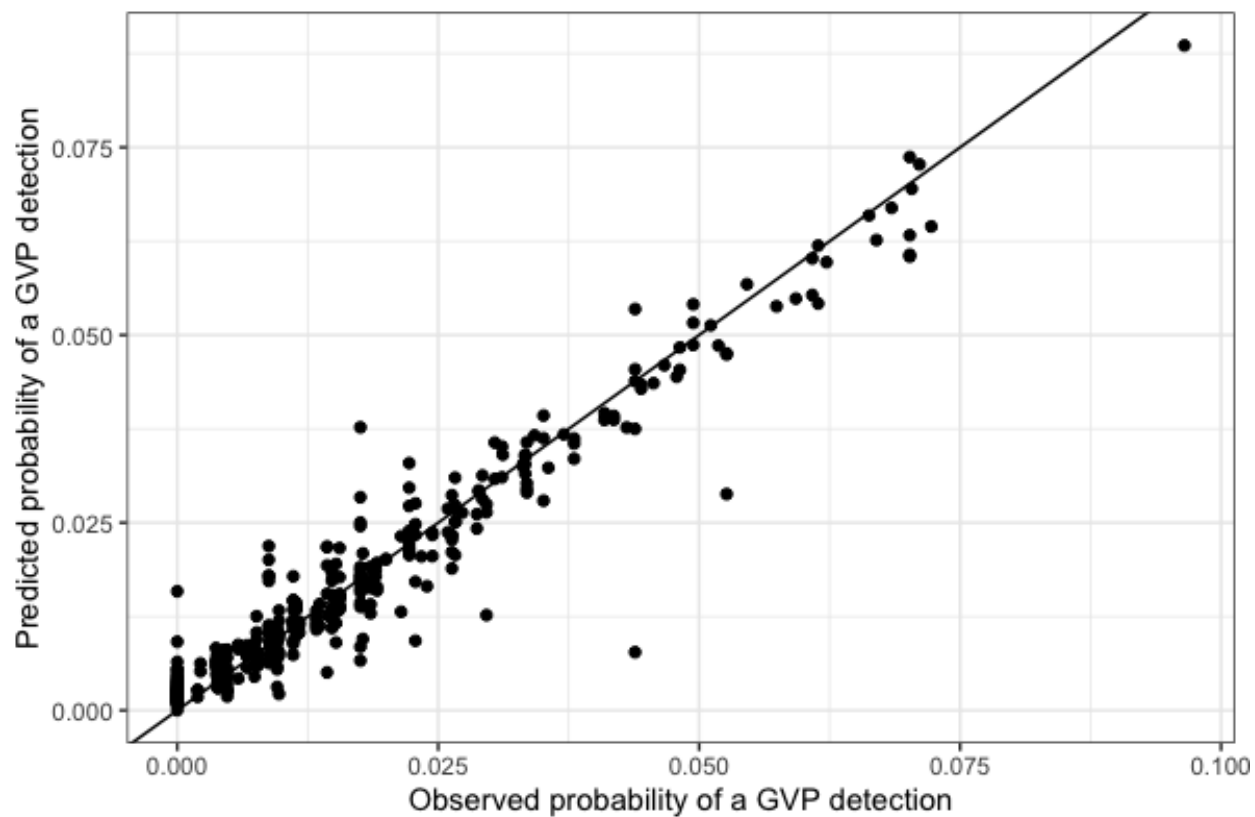


Figure S2.5: Observed (horizontal axis) versus M1 predicted (vertical axis) probability of detecting a GVP at each hydrophone during the baseline period.

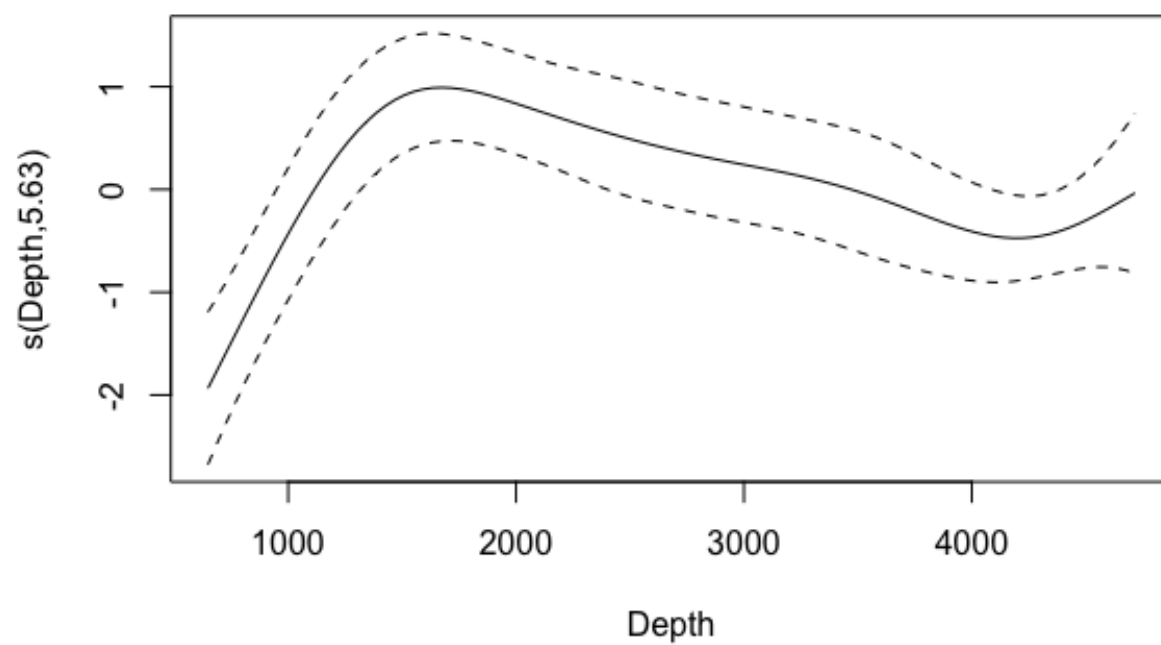


Figure S2.6: Spline on depth from M1.

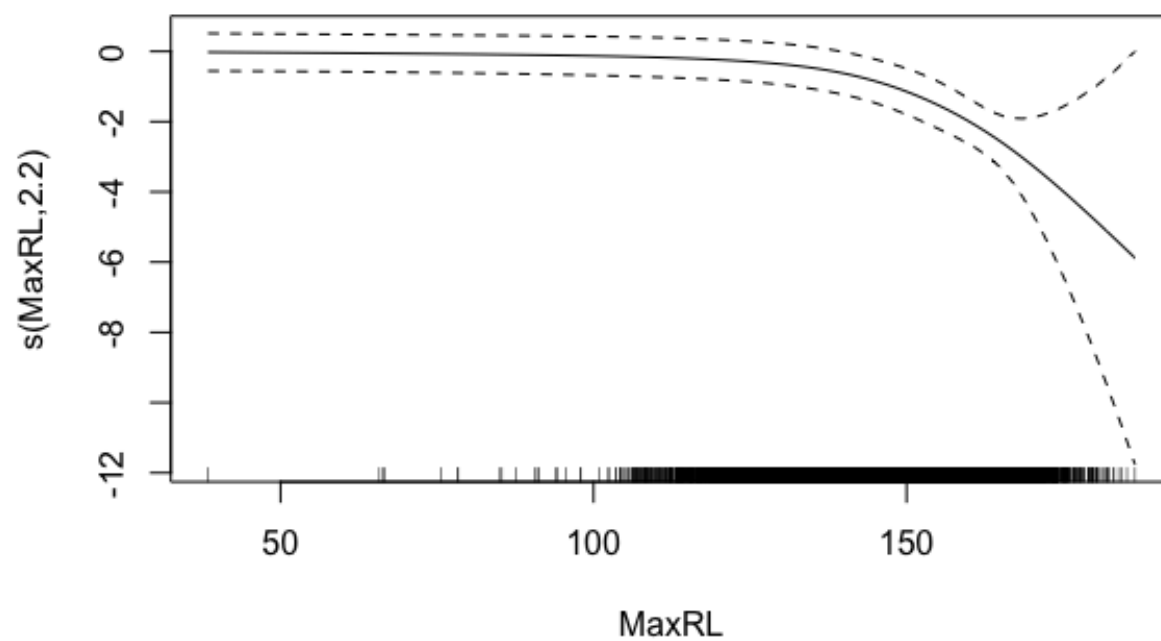


Figure S2.7: Spline on maximum received level from M3.

S3: Single GAM

A single GAM could be used to quantify the effect of naval sonar on Blainville’s beaked whales. Here, we present such a model and compare the results to the results obtained using the multi-stage model presented in the main text of the manuscript.

We modelled the probability of a GVP at tile i in SCC s at time t as a Bernoulli trial:

$\text{GVP}_{i,s,t} \sim \text{Bin}(1, \mu_{i,s,t})$. The linear predictor for on the logit scale was given as:

$$\text{logit}(\mu_{i,s,t}) = \beta_0 + \beta_1 \text{NavTrain}_t + f(\text{MRF}_{i,s}) + f(\text{Depth}_i) + f(\text{MaxRL}_{i,t}) \text{Sonar}_t + \log_e A_i$$

where β_0 is an intercept, $\beta_1 \text{NavTrain}_t$ is the effect of naval training times an indicator variable for whether naval training was present or absent at time t , $f(\text{MRF}_{i,s})$ denotes the Markov random field used to smooth space, $f(\text{Depth}_i)$ is a smooth of depth (using a thin plate spline; Wood et al. 2003), $f(\text{MaxRL}_{i,t}) \text{Sonar}_t$ is a monotonically decreasing smooth of sonar received level (using a thin plate spline) times an indicator variable for whether sonar was present or absent at time t , and $\log_e A_i$ is an offset for the area (in km^2) of each tile, A_i .

We fit the model using `scam` (Pya et al. 2015).

This single GAM predicts a 64% decrease in $\mathbb{P}(\text{GVP})$ when naval training is present compared to the baseline period, which is the same decrease predicted by the multi-stage GAM. However, the single GAM predicts that at a MFAS received level of 150 dB re 1 μPa , $\mathbb{P}(\text{GVP})$ will decrease by 64% relative to when only naval training is present, whereas the multi-stage model predicts a decrease of 78%. Similarly, the single GAM predicts that at a MFAS received level of 150 dB re 1 μPa , $\mathbb{P}(\text{GVP})$ will decrease by 87% relative to baseline, whereas the multi-stage model predicts a 92% decrease. Relative to when only naval training is present, the single GAM predicts a 50% reduction in $\mathbb{P}(\text{GVP})$ at a MFAS

received level of 144 dB, whereas the multi-stage model predicts a 50% reduction at a MFAS received level of 135 dB re 1 μ Pa.

The major difference between this single GAM and the multi-stage model presented in the main text of the manuscript is that here, the spatial smooth is constructed using data from the baseline, naval training, and MFAS periods of each SCC. Therefore, the spatial distribution of MFAS may influence the predicted distribution of Blainville's beaked whales. As expected, using a single GAM leads to underestimates of the impact of sonar, since changes in distribution due to MFAS are not captured by the MRF.

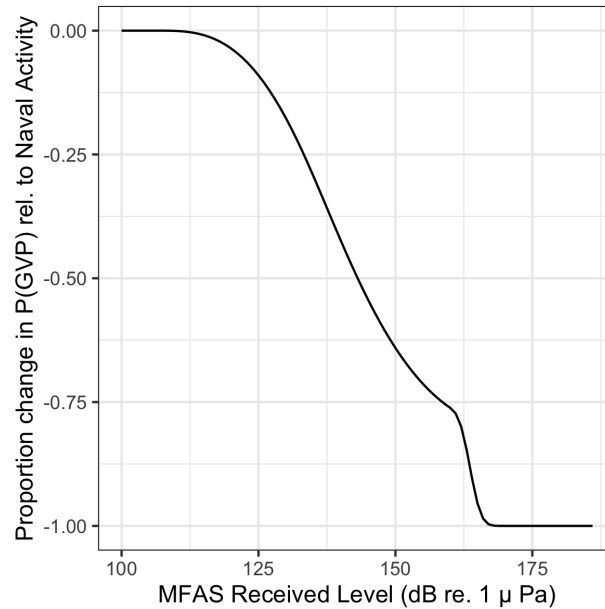


Figure S3.1: Results from a single GAM: Median (black line) expected change in the probability of detecting a group vocal period (vertical axis) with increasing MFAS received level (horizontal axis) relative to when naval training activity but no MFAS is present on the range.

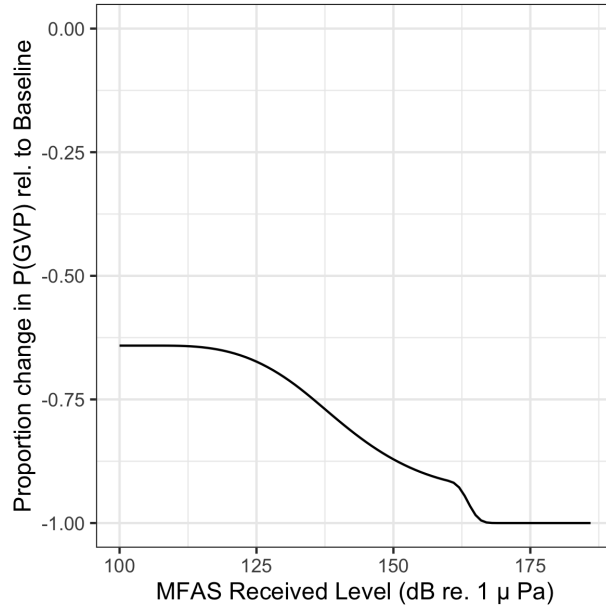


Figure S3.2: Results from a single GAM: Median (black line) expected change in the probability of detecting a group vocal period (vertical axis) with increasing MFAS received level (horizontal axis) relative to when neither naval training activity nor MFAS is present on the range.